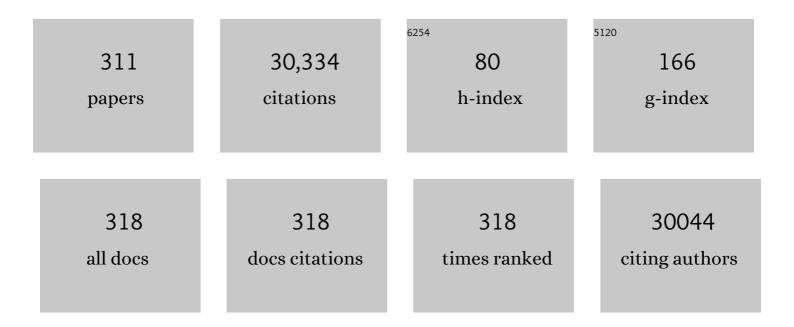
List of Publications by Year in descending order

Source: https://exaly.com/author-pdf/5516709/publications.pdf Version: 2024-02-01



#	Article	IF	CITATIONS
1	Highly Crystalline Multimetallic Nanoframes with Three-Dimensional Electrocatalytic Surfaces. Science, 2014, 343, 1339-1343.	12.6	2,376
2	Homogeneously dispersed multimetal oxygen-evolving catalysts. Science, 2016, 352, 333-337.	12.6	1,948
3	Structurally ordered intermetallic platinum–cobalt core–shell nanoparticles with enhanced activity and stability as oxygen reduction electrocatalysts. Nature Materials, 2013, 12, 81-87.	27.5	1,768
4	Memristors with diffusive dynamics as synaptic emulators for neuromorphic computing. Nature Materials, 2017, 16, 101-108.	27.5	1,655
5	Surface reconstruction and chemical evolution of stoichiometric layered cathode materials for lithium-ion batteries. Nature Communications, 2014, 5, 3529.	12.8	1,118
6	Evolution of redox couples in Li- and Mn-rich cathode materials and mitigation of voltage fade by reducing oxygen release. Nature Energy, 2018, 3, 690-698.	39.5	675
7	Atomically Dispersed Molybdenum Catalysts for Efficient Ambient Nitrogen Fixation. Angewandte Chemie - International Edition, 2019, 58, 2321-2325.	13.8	543
8	Theory-driven design of high-valence metal sites for water oxidation confirmed using in situ soft X-ray absorption. Nature Chemistry, 2018, 10, 149-154.	13.6	476
9	Facet development during platinum nanocube growth. Science, 2014, 345, 916-919.	12.6	429
10	Synchrotron X-ray Analytical Techniques for Studying Materials Electrochemistry in Rechargeable Batteries. Chemical Reviews, 2017, 117, 13123-13186.	47.7	390
11	Memristor crossbar arrays with 6-nm half-pitch and 2-nm critical dimension. Nature Nanotechnology, 2019, 14, 35-39.	31.5	381
12	Stable and Efficient Single-Atom Zn Catalyst for CO ₂ Reduction to CH ₄ . Journal of the American Chemical Society, 2020, 142, 12563-12567.	13.7	358
13	Diamond family of nanoparticle superlattices. Science, 2016, 351, 582-586.	12.6	331
14	A disordered rock salt anode for fast-charging lithium-ion batteries. Nature, 2020, 585, 63-67.	27.8	326
15	Amorphization activated ruthenium-tellurium nanorods for efficient waterÂsplitting. Nature Communications, 2019, 10, 5692.	12.8	312
16	Visualization of Electrode–Electrolyte Interfaces in LiPF ₆ /EC/DEC Electrolyte for Lithium Ion Batteries via in Situ TEM. Nano Letters, 2014, 14, 1745-1750.	9.1	304
17	Pt-Decorated PdCo@Pd/C Coreâ^'Shell Nanoparticles with Enhanced Stability and Electrocatalytic Activity for the Oxygen Reduction Reaction. Journal of the American Chemical Society, 2010, 132, 17664-17666.	13.7	300
18	Anatomy of Ag/Hafniaâ€Based Selectors with 10 ¹⁰ Nonlinearity. Advanced Materials, 2017, 29, 1604457.	21.0	292

#	Article	IF	CITATIONS
19	Tuning Oxygen Reduction Reaction Activity via Controllable Dealloying: A Model Study of Ordered Cu ₃ Pt/C Intermetallic Nanocatalysts. Nano Letters, 2012, 12, 5230-5238.	9.1	291
20	In Situ STEM-EELS Observation of Nanoscale Interfacial Phenomena in All-Solid-State Batteries. Nano Letters, 2016, 16, 3760-3767.	9.1	278
21	Solutionâ€Processable Glass Lilâ€Li ₄ SnS ₄ Superionic Conductors for Allâ€Solidâ€State Liâ€Ion Batteries. Advanced Materials, 2016, 28, 1874-1883.	21.0	265
22	Visualizing the 3D Internal Structure of Calcite Single Crystals Grown in Agarose Hydrogels. Science, 2009, 326, 1244-1247.	12.6	257
23	Surface patterning of nanoparticles with polymer patches. Nature, 2016, 538, 79-83.	27.8	257
24	Recent Advances of Structurally Ordered Intermetallic Nanoparticles for Electrocatalysis. ACS Catalysis, 2018, 8, 3237-3256.	11.2	245
25	Prescribed nanoparticle cluster architectures and low-dimensional arrays built using octahedral DNA origami frames. Nature Nanotechnology, 2015, 10, 637-644.	31.5	243
26	Oxygen Release Induced Chemomechanical Breakdown of Layered Cathode Materials. Nano Letters, 2018, 18, 3241-3249.	9.1	237
27	Sub-50-nm self-assembled nanotextures for enhanced broadband antireflection in silicon solar cells. Nature Communications, 2015, 6, 5963.	12.8	230
28	Porous Structured Ni–Fe–P Nanocubes Derived from a Prussian Blue Analogue as an Electrocatalyst for Efficient Overall Water Splitting. ACS Applied Materials & Interfaces, 2017, 9, 26134-26142.	8.0	220
29	Metal segregation in hierarchically structured cathode materials for high-energy lithiumÂbatteries. Nature Energy, 2016, 1, .	39.5	209
30	Promoting H2O2 production via 2-electron oxygen reduction by coordinating partially oxidized Pd with defect carbon. Nature Communications, 2020, 11, 2178.	12.8	209
31	Lattice engineering through nanoparticle–DNA frameworks. Nature Materials, 2016, 15, 654-661.	27.5	198
32	Bimetallic synergy in cobalt–palladium nanocatalysts for CO oxidation. Nature Catalysis, 2019, 2, 78-85.	34.4	195
33	Superlattices assembled through shape-induced directional binding. Nature Communications, 2015, 6, 6912.	12.8	188
34	Effect of biaxial strain on the electrical and magnetic properties of (001) La0.7Sr0.3MnO3 thin films. Applied Physics Letters, 2009, 95, .	3.3	184
35	Altering Ligand Fields in Single-Atom Sites through Second-Shell Anion Modulation Boosts the Oxygen Reduction Reaction. Journal of the American Chemical Society, 2022, 144, 2197-2207.	13.7	183
36	Sub-10 nm Ta Channel Responsible for Superior Performance of a HfO2 Memristor. Scientific Reports, 2016, 6, 28525.	3.3	177

#	Article	IF	CITATIONS
37	A spongy nickel-organic CO ₂ reduction photocatalyst for nearly 100% selective CO production. Science Advances, 2017, 3, e1700921.	10.3	175
38	Ordered three-dimensional nanomaterials using DNA-prescribed and valence-controlled material voxels. Nature Materials, 2020, 19, 789-796.	27.5	172
39	Profiling the nanoscale gradient in stoichiometric layered cathode particles for lithium-ion batteries. Energy and Environmental Science, 2014, 7, 3077.	30.8	170
40	Aperture-scanning Fourier ptychography for 3D refocusing and super-resolution macroscopic imaging. Optics Express, 2014, 22, 13586.	3.4	166
41	Polymorph Evolution Mechanisms and Regulation Strategies of Lithium Metal Anode under Multiphysical Fields. Chemical Reviews, 2021, 121, 5986-6056.	47.7	165
42	Facile Synthesis of Carbon-Supported Pd–Co Core–Shell Nanoparticles as Oxygen Reduction Electrocatalysts and Their Enhanced Activity and Stability with Monolayer Pt Decoration. Chemistry of Materials, 2012, 24, 2274-2281.	6.7	163
43	Phase evolution for conversion reaction electrodes in lithium-ion batteries. Nature Communications, 2014, 5, 3358.	12.8	163
44	Three-Dimensional Tracking and Visualization of Hundreds of Ptâ^'Co Fuel Cell Nanocatalysts During Electrochemical Aging. Nano Letters, 2012, 12, 4417-4423.	9.1	162
45	Revealing the Atomic Restructuring of Pt–Co Nanoparticles. Nano Letters, 2014, 14, 3203-3207.	9.1	162
46	Atomic-Resolution Spectroscopic Imaging of Ensembles of Nanocatalyst Particles Across the Life of a Fuel Cell. Nano Letters, 2012, 12, 490-497.	9.1	161
47	Fluorine-Anion-Modulated Electron Structure of Nickel Sulfide Nanosheet Arrays for Alkaline Hydrogen Evolution. ACS Energy Letters, 2019, 4, 2905-2912.	17.4	159
48	Three-dimensional crossbar arrays of self-rectifying Si/SiO2/Si memristors. Nature Communications, 2017, 8, 15666.	12.8	153
49	Regioselective surface encoding of nanoparticles for programmable self-assembly. Nature Materials, 2019, 18, 169-174.	27.5	153
50	Modulating Singleâ€Atom Palladium Sites with Copper for Enhanced Ambient Ammonia Electrosynthesis. Angewandte Chemie - International Edition, 2021, 60, 345-350.	13.8	150
51	A single-atom library for guided monometallic and concentration-complex multimetallic designs. Nature Materials, 2022, 21, 681-688.	27.5	145
52	Constructing FeN4/graphitic nitrogen atomic interface for high-efficiency electrochemical CO2 reduction over a broad potential window. CheM, 2021, 7, 1297-1307.	11.7	133
53	Facet Control of Gold Nanorods. ACS Nano, 2016, 10, 2960-2974.	14.6	131
54	Ultrahighâ€Rate and Longâ€Life Zinc–Metal Anodes Enabled by Selfâ€Accelerated Cation Migration. Advanced Energy Materials, 2021, 11, 2100982.	19.5	131

#	Article	IF	CITATIONS
55	One-Nanometer-Thick Pt ₃ Ni Bimetallic Alloy Nanowires Advanced Oxygen Reduction Reaction: Integrating Multiple Advantages into One Catalyst. ACS Catalysis, 2019, 9, 4488-4494.	11.2	126
56	Depth-Dependent Redox Behavior of LiNi _{0.6} Mn _{0.2} Co _{0.2} O ₂ . Journal of the Electrochemical Society, 2018, 165, A696-A704.	2.9	123
57	Sodiation Kinetics of Metal Oxide Conversion Electrodes: A Comparative Study with Lithiation. Nano Letters, 2015, 15, 5755-5763.	9.1	122
58	Trifunctional Singleâ€Atomic Ru Sites Enable Efficient Overall Water Splitting and Oxygen Reduction in Acidic Media. Small, 2020, 16, e2002888.	10.0	120
59	Mesoporous CNT@TiO2-C Nanocable with Extremely Durable High Rate Capability for Lithium-Ion Battery Anodes. Scientific Reports, 2014, 4, 3729.	3.3	116
60	In Situ Observation of Oscillatory Growth of Bismuth Nanoparticles. Nano Letters, 2012, 12, 1470-1474.	9.1	114
61	Self-assembled V2O5 nanosheets/reduced graphene oxide hierarchical nanocomposite as a high-performance cathode material for lithium ion batteries. Journal of Materials Chemistry A, 2013, 1, 10814.	10.3	114
62	From a ZIF-8 polyhedron to three-dimensional nitrogen doped hierarchical porous carbon: an efficient electrocatalyst for the oxygen reduction reaction. Journal of Materials Chemistry A, 2018, 6, 10731-10739.	10.3	111
63	Deciphering the Cathode–Electrolyte Interfacial Chemistry in Sodium Layered Cathode Materials. Advanced Energy Materials, 2018, 8, 1801975.	19.5	111
64	Dopant Distribution in Co-Free High-Energy Layered Cathode Materials. Chemistry of Materials, 2019, 31, 9769-9776.	6.7	110
65	Block Copolymer Self-Assembly–Directed Single-Crystal Homo- and Heteroepitaxial Nanostructures. Science, 2010, 330, 214-219.	12.6	108
66	Chemical and Structural Stability of Lithium-Ion Battery Electrode Materials under Electron Beam. Scientific Reports, 2014, 4, 5694.	3.3	108
67	Calcite Prisms from Mollusk Shells (<i>Atrina Rigida</i>): Swissâ€cheeseâ€like Organic–Inorganic Singleâ€crystal Composites. Advanced Functional Materials, 2011, 21, 2028-2034.	14.9	104
68	Data Processing for Atomic Resolution Electron Energy Loss Spectroscopy. Microscopy and Microanalysis, 2012, 18, 667-675.	0.4	103
69	Coupled s-p-d Exchange in Facet-Controlled Pd3Pb Tripods Enhances Oxygen Reduction Catalysis. CheM, 2018, 4, 359-371.	11.7	100
70	Optimizing the ORR activity of Pd based nanocatalysts by tuning their strain and particle size. Journal of Materials Chemistry A, 2017, 5, 9867-9872.	10.3	98
71	Heteroatom (P, B, or S) incorporated NiFe-based nanocubes as efficient electrocatalysts for the oxygen evolution reaction. Journal of Materials Chemistry A, 2018, 6, 7062-7069.	10.3	98
72	High-Performance Nitrogen-Doped Intermetallic PtNi Catalyst for the Oxygen Reduction Reaction. ACS Catalysis, 2020, 10, 10637-10645.	11.2	98

#	Article	IF	CITATIONS
73	Transitions from Near-Surface to Interior Redox upon Lithiation in Conversion Electrode Materials. Nano Letters, 2015, 15, 1437-1444.	9.1	97
74	Atomically Dispersed Molybdenum Catalysts for Efficient Ambient Nitrogen Fixation. Angewandte Chemie, 2019, 131, 2343-2347.	2.0	95
75	Local Modulation of Single-Atomic Mn Sites for Enhanced Ambient Ammonia Electrosynthesis. ACS Catalysis, 2021, 11, 509-516.	11.2	93
76	One-pot synthesis of carbon coated-SnO2/graphene-sheet nanocomposite with highly reversible lithium storage capability. Journal of Power Sources, 2013, 232, 152-158.	7.8	91
77	Liquid-Like, Self-Healing Aluminum Oxide during Deformation at Room Temperature. Nano Letters, 2018, 18, 2492-2497.	9.1	91
78	Comparison between Dealloyed PtCo ₃ and PtCu ₃ Cathode Catalysts for Proton Exchange Membrane Fuel Cells. Journal of Physical Chemistry C, 2012, 116, 19877-19885.	3.1	90
79	Design of Ru-Ni diatomic sites for efficient alkaline hydrogen oxidation. Science Advances, 2022, 8, .	10.3	89
80	Revealing Correlation of Valence State with Nanoporous Structure in Cobalt Catalyst Nanoparticles by <i>In Situ</i> Environmental TEM. ACS Nano, 2012, 6, 4241-4247.	14.6	84
81	Electronic Tuning of Metal Nanoparticles for Highly Efficient Photocatalytic Hydrogen Peroxide Production. ACS Catalysis, 2019, 9, 626-631.	11.2	84
82	Effects of cathode electrolyte interfacial (CEI) layer on long term cycling of all-solid-state thin-film batteries. Journal of Power Sources, 2016, 324, 342-348.	7.8	82
83	Garnet Electrolyte Surface Degradation and Recovery. ACS Applied Energy Materials, 2018, 1, 7244-7252.	5.1	81
84	Structure evolution of PtCu nanoframes from disordered to ordered for the oxygen reduction reaction. Applied Catalysis B: Environmental, 2021, 282, 119617.	20.2	80
85	SnS2 nanoparticle loaded graphene nanocomposites for superior energy storage. Physical Chemistry Chemical Physics, 2012, 14, 6981.	2.8	79
86	Aberration-corrected ADF-STEM depth sectioning and prospects for reliable 3D imaging in S/TEM. Journal of Electron Microscopy, 2009, 58, 157-165.	0.9	77
87	Recent Progress on Mesoporous Carbon Materials for Advanced Energy Conversion and Storage. Particle and Particle Systems Characterization, 2014, 31, 515-539.	2.3	77
88	Tailoring the Antipoisoning Performance of Pd for Formic Acid Electrooxidation via an Ordered PdBi Intermetallic. ACS Catalysis, 2020, 10, 9977-9985.	11.2	75
89	Characterization of the structure and chemistry of the solid–electrolyte interface by cryo-EM leads to high-performance solid-state Li-metal batteries. Nature Nanotechnology, 2022, 17, 768-776.	31.5	75
90	Supramolecular gel-assisted synthesis of double shelled Co@CoO@N–C/C nanoparticles with synergistic electrocatalytic activity for the oxygen reduction reaction. Nanoscale, 2016, 8, 4681-4687.	5.6	74

#	Article	IF	CITATIONS
91	Activating Edge-Mo of 2H-MoS ₂ <i>via</i> Coordination with Pyridinic N–C for pH-Universal Hydrogen Evolution Electrocatalysis. ACS Catalysis, 2021, 11, 4486-4497.	11.2	74
92	Sulphur modulated Ni3FeN supported on N/S co-doped graphene boosts rechargeable/flexible Zn-air battery performance. Applied Catalysis B: Environmental, 2020, 274, 119086.	20.2	73
93	Coalescence in the Thermal Annealing of Nanoparticles: An in Situ STEM Study of the Growth Mechanisms of Ordered Pt–Fe Nanoparticles in a KCl Matrix. Chemistry of Materials, 2013, 25, 1436-1442.	6.7	72
94	<i>In Situ</i> TEM Study of Catalytic Nanoparticle Reactions in Atmospheric Pressure Gas Environment. Microscopy and Microanalysis, 2013, 19, 1558-1568.	0.4	72
95	Giant Magnetoresistive Phosphoric Acid Doped Polyaniline–Silica Nanocomposites. Journal of Physical Chemistry C, 2013, 117, 6426-6436.	3.1	70
96	Hollowâ€Structured Carbonâ€Supported Nickel Cobaltite Nanoparticles as an Efficient Bifunctional Electrocatalyst for the Oxygen Reduction and Evolution Reactions. ChemCatChem, 2016, 8, 736-742.	3.7	70
97	Single-Atom Pt Catalyst for Effective C–F Bond Activation via Hydrodefluorination. ACS Catalysis, 2018, 8, 9353-9358.	11.2	70
98	Resolving atomic-scale phase transformation and oxygen loss mechanism in ultrahigh-nickel layered cathodes for cobalt-free lithium-ion batteries. Matter, 2021, 4, 2013-2026.	10.0	69
99	Spontaneous incorporation of gold in palladium-based ternary nanoparticles makes durable electrocatalysts for oxygen reduction reaction. Nature Communications, 2016, 7, 11941.	12.8	67
100	Nitrogen and sulfur co-doping of partially exfoliated MWCNTs as 3-D structured electrocatalysts for the oxygen reduction reaction. Journal of Materials Chemistry A, 2016, 4, 5678-5684.	10.3	66
101	Effects of crystal phase and composition on structurally ordered Pt–Co–Ni/C ternary intermetallic electrocatalysts for the formic acid oxidation reaction. Journal of Materials Chemistry A, 2018, 6, 5848-5855.	10.3	66
102	Atomic rearrangement from disordered to ordered Pd-Fe nanocatalysts with trace amount of Pt decoration for efficient electrocatalysis. Nano Energy, 2018, 50, 70-78.	16.0	66
103	Solutionâ€Grown Organic Singleâ€Crystalline Donor–Acceptor Heterojunctions for Photovoltaics. Angewandte Chemie - International Edition, 2015, 54, 956-960.	13.8	65
104	Interrogation of bimetallic particle oxidation in three dimensions at the nanoscale. Nature Communications, 2016, 7, 13335.	12.8	65
105	Direct high-resolution mapping of electrocatalytic activity of semi-two-dimensional catalysts with single-edge sensitivity. Proceedings of the National Academy of Sciences of the United States of America, 2019, 116, 11618-11623.	7.1	65
106	Collective Plasmon Coupling in Gold Nanoparticle Clusters for Highly Efficient Photothermal Therapy. ACS Nano, 2022, 16, 910-920.	14.6	65
107	Explore the Effects of Microstructural Defects on Voltage Fade of Li- and Mn-Rich Cathodes. Nano Letters, 2016, 16, 5999-6007.	9.1	64
108	Boosting the electron mobility of solution-grown organic single crystals via reducing the amount of polar solvent residues. Materials Horizons, 2016, 3, 119-123.	12.2	64

#	Article	IF	CITATIONS
109	Self-Optimized Ligand Effect in L1 ₂ -PtPdFe Intermetallic for Efficient and Stable Alkaline Hydrogen Oxidation Reaction. ACS Catalysis, 2020, 10, 15207-15216.	11.2	64
110	Shape-Specific Patterning of Polymer-Functionalized Nanoparticles. ACS Nano, 2017, 11, 4995-5002.	14.6	63
111	Analytic derivation of optimal imaging conditions for incoherent imaging in aberration-corrected electron microscopes. Ultramicroscopy, 2008, 108, 1454-1466.	1.9	62
112	An electrochemically stable homogeneous glassy electrolyte formed at room temperature for all-solid-state sodium batteries. Nature Communications, 2022, 13, .	12.8	62
113	Synergistic enhancement of nitrogen and sulfur co-doped graphene with carbon nanosphere insertion for the electrocatalytic oxygen reduction reaction. Journal of Materials Chemistry A, 2015, 3, 7727-7731.	10.3	61
114	Anomalous metal segregation in lithium-rich material provides design rules for stable cathode in lithium-ion battery. Nature Communications, 2019, 10, 1650.	12.8	60
115	Ambipolar charge transport of TIPS-pentacene single-crystals grown from non-polar solvents. Materials Horizons, 2015, 2, 344-349.	12.2	59
116	Nitrogen-doped carbon nanofibers derived from polypyrrole coated bacterial cellulose as high-performance electrode materials for supercapacitors and Li-ion batteries. Electrochimica Acta, 2016, 210, 130-137.	5.2	59
117	Spinel Ferrite Core–Shell Nanostructures by a Versatile Solvothermal Seed-Mediated Growth Approach and Study of Their Nanointerfaces. ACS Nano, 2017, 11, 7889-7900.	14.6	59
118	Hierarchical nickel valence gradient stabilizes high-nickel content layered cathode materials. Nature Communications, 2021, 12, 2350.	12.8	59
119	Probing microstructure and phase evolution of $\hat{1}\pm$ -MoO3 nanobelts for sodium-ion batteries by in situ transmission electron microscopy. Nano Energy, 2016, 27, 447-456.	16.0	58
120	Composition-dependent electrocatalytic activities of NiFe-based selenides for the oxygen evolution reaction. Electrochimica Acta, 2018, 291, 64-72.	5.2	58
121	Atomic-resolution spectroscopic imaging of oxide interfaces. Philosophical Magazine, 2010, 90, 4731-4749.	1.6	57
122	In situ TEM probing of crystallization form-dependent sodiation behavior in ZnO nanowires for sodium-ion batteries. Nano Energy, 2016, 30, 771-779.	16.0	57
123	FeMo sub-nanoclusters/single atoms for neutral ammonia electrosynthesis. Nano Energy, 2020, 77, 105078.	16.0	56
124	Depth sectioning of individual dopant atoms with aberration-corrected scanning transmission electron microscopy. Applied Physics Letters, 2008, 92, .	3.3	55
125	Epitaxial Bi ₅ Ti ₃ FeO ₁₅ –CoFe ₂ O ₄ Pillar–Matrix Multiferroic Nanostructures. ACS Nano, 2013, 7, 11079-11086.	14.6	55
126	Stabilizing and Activating Metastable Nickel Nanocrystals for Highly Efficient Hydrogen Evolution Electrocatalysis. ACS Nano, 2018, 12, 11625-11631.	14.6	55

#	Article	IF	CITATIONS
127	Combining structurally ordered intermetallics with N-doped carbon confinement for efficient and anti-poisoning electrocatalysis. Applied Catalysis B: Environmental, 2020, 279, 119370.	20.2	55
128	TEMImageNet training library and AtomSegNet deep-learning models for high-precision atom segmentation, localization, denoising, and deblurring of atomic-resolution images. Scientific Reports, 2021, 11, 5386.	3.3	55
129	Three-dimensional hollow-structured binary oxide particles as an advanced anode material for high-rate and long cycle life lithium-ion batteries. Nano Energy, 2016, 20, 212-220.	16.0	53
130	Electrolyte Regulating toward Stabilization of Cobalt-Free Ultrahigh-Nickel Layered Oxide Cathode in Lithium-Ion Batteries. ACS Energy Letters, 2021, 6, 1324-1332.	17.4	53
131	Nanoparticles Incorporated inside Single-Crystals: Enhanced Fluorescent Properties. Chemistry of Materials, 2016, 28, 7537-7543.	6.7	52
132	Accelerated Evolution of Surface Chemistry Determined by Temperature and Cycling History in Nickel-Rich Layered Cathode Materials. ACS Applied Materials & Interfaces, 2018, 10, 23842-23850.	8.0	52
133	One-Pot Synthesis of B/P-Codoped Co-Mo Dual-Nanowafer Electrocatalysts for Overall Water Splitting. ACS Applied Materials & Interfaces, 2021, 13, 20024-20033.	8.0	52
134	Rational design of three-dimensional nitrogen and phosphorus co-doped graphene nanoribbons/CNTs composite for the oxygen reduction. Chinese Chemical Letters, 2016, 27, 597-601.	9.0	51
135	Collisions of Ir Oxide Nanoparticles with Carbon Nanopipettes: Experiments with One Nanoparticle. Analytical Chemistry, 2017, 89, 2880-2885.	6.5	51
136	MCM-41 support for ultrasmall γ-Fe ₂ O ₃ nanoparticles for H ₂ S removal. Journal of Materials Chemistry A, 2017, 5, 21688-21698.	10.3	51
137	A joint deep learning model to recover information and reduce artifacts in missing-wedge sinograms for electron tomography and beyond. Scientific Reports, 2019, 9, 12803.	3.3	51
138	Rhombohedral Ordered Intermetallic Nanocatalyst Boosts the Oxygen Reduction Reaction. ACS Catalysis, 2021, 11, 184-192.	11.2	51
139	Controllable construction of flower-like FeS/Fe2O3 composite for lithium storage. Journal of Power Sources, 2018, 392, 193-199.	7.8	50
140	Sub-nm ruthenium cluster as an efficient and robust catalyst for decomposition and synthesis of ammonia: Break the "size shackles― Nano Research, 2018, 11, 4774-4785.	10.4	49
141	Bimetallic Nanoparticle Oxidation in Three Dimensions by Chemically Sensitive Electron Tomography and <i>in Situ</i> Transmission Electron Microscopy. ACS Nano, 2018, 12, 7866-7874.	14.6	49
142	Interfacing Solutionâ€Grown C ₆₀ and (3â€Pyrrolinium)(CdCl ₃) Single Crystals for Highâ€Mobility Transistorâ€Based Memory Devices. Advanced Materials, 2015, 27, 4476-4480.	21.0	48
143	3D hollow structured Co ₂ FeO ₄ /MWCNT as an efficient non-precious metal electrocatalyst for oxygen reduction reaction. Journal of Materials Chemistry A, 2015, 3, 1601-1608.	10.3	48
144	Atomically Isolated Rh Sites within Highly Branched Rh ₂ Sb Nanostructures Enhance Bifunctional Hydrogen Electrocatalysis. Advanced Materials, 2021, 33, e2105049.	21.0	48

#	Article	IF	CITATIONS
145	Nanostructured flexible Mg-modified LiMnPO ₄ matrix as high-rate cathode materials for Li-ion batteries. Journal of Materials Chemistry A, 2014, 2, 6368-6373.	10.3	47
146	A closer look at the physical and optical properties of gold nanostars: an experimental and computational study. Nanoscale, 2017, 9, 3766-3773.	5.6	47
147	Creating compressive stress at the NiOOH/NiO interface for water oxidation. Journal of Materials Chemistry A, 2020, 8, 10747-10754.	10.3	47
148	Conformal coating of TiO2 nanorods on a 3-D CNT scaffold by using a CNT film as a nanoreactor: a free-standing and binder-free Li-ion anode. Journal of Materials Chemistry A, 2014, 2, 2701.	10.3	46
149	Structurally ordered Pt–Zn/C series nanoparticles as efficient anode catalysts for formic acid electrooxidation. Journal of Materials Chemistry A, 2015, 3, 22129-22135.	10.3	46
150	Elucidating the Limit of Li Insertion into the Spinel Li ₄ Ti ₅ O ₁₂ . , 2019, 1, 96-102.		45
151	Extended Depth of Field for High-Resolution Scanning Transmission Electron Microscopy. Microscopy and Microanalysis, 2011, 17, 75-80.	0.4	44
152	A New Anion Receptor for Improving the Interface between Lithium- and Manganese-Rich Layered Oxide Cathode and the Electrolyte. Chemistry of Materials, 2017, 29, 2141-2149.	6.7	44
153	Selective Electrocatalytic Reduction of CO ₂ into CO at Small, Thiol-Capped Au/Cu Nanoparticles. Journal of Physical Chemistry C, 2018, 122, 27991-28000.	3.1	44
154	Enhancing surface oxygen retention through theory-guided doping selection in Li _{1â^x} NiO ₂ for next-generation lithium-ion batteries. Journal of Materials Chemistry A, 2020, 8, 23293-23303.	10.3	44
155	Highly active N-doped carbon encapsulated Pd-Fe intermetallic nanoparticles for the oxygen reduction reaction. Nano Research, 2020, 13, 2365-2370.	10.4	44
156	Modulating Singleâ€Atom Palladium Sites with Copper for Enhanced Ambient Ammonia Electrosynthesis. Angewandte Chemie, 2021, 133, 349-354.	2.0	44
157	Highly Selective Oxygen Reduction to Hydrogen Peroxide on a Carbon-Supported Single-Atom Pd Electrocatalyst. ACS Catalysis, 2022, 12, 4156-4164.	11.2	44
158	Selective Placement of Faceted Metal Tips on Semiconductor Nanorods. Angewandte Chemie - International Edition, 2013, 52, 980-982.	13.8	43
159	Influence of synthesis conditions on the surface passivation and electrochemical behavior of layered cathode materials. Journal of Materials Chemistry A, 2014, 2, 19833-19840.	10.3	43
160	Atomic-Scale Observation of O1 Faulted Phase-Induced Deactivation of LiNiO ₂ at High Voltage. Nano Letters, 2021, 21, 3657-3663.	9.1	43
161	Three-Dimensional Patterning of Nanoparticles by Molecular Stamping. ACS Nano, 2020, 14, 6823-6833.	14.6	42
162	Tuning the electrocatalytic activity of Pt by structurally ordered PdFe/C for the hydrogen oxidation reaction in alkaline media, Journal of Materials Chemistry A, 2018, 6, 11346-11352	10.3	41

#	Article	IF	CITATIONS
163	In situ visualization of sodium transport and conversion reactions of FeS2 nanotubes made by morphology engineering. Nano Energy, 2019, 60, 424-431.	16.0	41
164	The sensitive surface chemistry of Co-free, Ni-rich layered oxides: identifying experimental conditions that influence characterization results. Journal of Materials Chemistry A, 2020, 8, 17487-17497.	10.3	41
165	High-rate and long-life lithium-ion battery performance of hierarchically hollow-structured NiCo2O4/CNT nanocomposite. Electrochimica Acta, 2017, 244, 8-15.	5.2	39
166	Electronic structure and oxophilicity optimization of mono-layer Pt for efficient electrocatalysis. Nano Energy, 2020, 74, 104877.	16.0	39
167	Compositionâ€Tunable Antiperovskite Cu _{<i>x</i>} In _{1â^²<i>x</i>} NNi ₃ as Superior Electrocatalysts for the Hydrogen Evolution Reaction. Angewandte Chemie - International Edition, 2020, 59, 17488-17493.	13.8	39
168	Chemomechanically Stable Ultrahigh-Ni Single-Crystalline Cathodes with Improved Oxygen Retention and Delayed Phase Degradations. Nano Letters, 2021, 21, 9797-9804.	9.1	38
169	Valence-programmable nanoparticle architectures. Nature Communications, 2020, 11, 2279.	12.8	37
170	Diatomiteâ€Derived Hierarchical Porous Crystallineâ€AmorphousNetwork for Highâ€Performance and Sustainable Si Anodes. Advanced Functional Materials, 2020, 30, 2005956.	14.9	36
171	Deterministic arbitrary switching of polarization in a ferroelectric thin film. Nature Communications, 2014, 5, 4971.	12.8	35
172	Amorphous Lithium Lanthanum Titanate for Solid-State Microbatteries. Journal of the Electrochemical Society, 2017, 164, A6268-A6273.	2.9	35
173	Anomalous Conductivity Tailored by Domain-Boundary Transport in Crystalline Bismuth Vanadate Photoanodes. Chemistry of Materials, 2018, 30, 1677-1685.	6.7	35
174	Polarizationâ€Modulated Multidirectional Photothermal Actuators. Advanced Materials, 2021, 33, e2006367.	21.0	35
175	Three-Dimensional Atomic Structure of Grain Boundaries Resolved by Atomic-Resolution Electron Tomography. Matter, 2020, 3, 1999-2011.	10.0	34
176	Three-Dimensional Imaging in Aberration-Corrected Electron Microscopes. Microscopy and Microanalysis, 2010, 16, 445-455.	0.4	33
177	Ultrasensitive Detection of Dopamine with Carbon Nanopipets. Analytical Chemistry, 2019, 91, 12935-12941.	6.5	33
178	Targeted Surface Doping with Reversible Local Environment Improves Oxygen Stability at the Electrochemical Interfaces of Nickel-Rich Cathode Materials. ACS Applied Materials & Interfaces, 2019, 11, 37885-37891.	8.0	33
179	Optimizing PtFe intermetallics for oxygen reduction reaction: from DFT screening to <i>in situ</i> XAFS characterization. Nanoscale, 2019, 11, 20301-20306.	5.6	33
180	Supra-Nanoparticle Functional Assemblies through Programmable Stacking. ACS Nano, 2017, 11, 7036-7048.	14.6	32

#	Article	IF	CITATIONS
181	Coupled hard–soft spinel ferrite-based core–shell nanoarchitectures: magnetic properties and heating abilities. Nanoscale Advances, 2020, 2, 3191-3201.	4.6	32
182	Organic Heterojunctions Formed by Interfacing Two Single Crystals from a Mixed Solution. Journal of the American Chemical Society, 2019, 141, 10007-10015.	13.7	31
183	Optimizing electron density of nickel sulfide electrocatalysts through sulfur vacancy engineering for alkaline hydrogen evolution. Journal of Materials Chemistry A, 2020, 8, 18207-18214.	10.3	31
184	Accelerated Degradation in a Quasi-Single-Crystalline Layered Oxide Cathode for Lithium-Ion Batteries Caused by Residual Grain Boundaries. Nano Letters, 2022, 22, 3818-3824.	9.1	31
185	Supercluster-coupled crystal growth in metallic glass forming liquids. Nature Communications, 2019, 10, 915.	12.8	30
186	Structural Degradation of Layered Cathode Materials in Lithium-Ion Batteries Induced by Ball Milling. Journal of the Electrochemical Society, 2019, 166, A1964-A1971.	2.9	28
187	Conversion of CO ₂ on a highly active and stable Cu/FeO _x /CeO ₂ catalyst: tuning catalytic performance by oxide-oxide interactions. Catalysis Science and Technology, 2019, 9, 3735-3742.	4.1	28
188	Is there a Stobbs factor in atomic-resolution STEM-EELS mapping?. Ultramicroscopy, 2014, 139, 38-46.	1.9	27
189	Surface engineering of PdFe ordered intermetallics for efficient oxygen reduction electrocatalysis. Chemical Engineering Journal, 2021, 408, 127297.	12.7	27
190	Multicolor Photonic Pigments for Rotationâ€Asymmetric Mechanochromic Devices. Advanced Materials, 2022, 34, e2107398.	21.0	27
191	Atomic-Scale Compositional Mapping and 3-Dimensional Electron Microscopy of Dealloyed PtCo3Catalyst Nanoparticles with Spongy Multi-Core/Shell Structures. Journal of the Electrochemical Society, 2012, 159, F554-F559.	2.9	26
192	Ultralow content of Pt on Pd–Co–Cu/C ternary nanoparticles with excellent electrocatalytic activity and durability for the oxygen reduction reaction. Nano Energy, 2016, 27, 475-481.	16.0	26
193	Modulating the Electronic Structure of Nickel Sulfide Electrocatalysts by Chlorine Doping toward Highly Efficient Alkaline Hydrogen Evolution. ACS Applied Materials & Interfaces, 2022, 14, 6869-6875.	8.0	25
194	On-Column 2 <i>p</i> Bound State with Topological Charge ±1 Excited by an Atomic-Size Vortex Beam in an Aberration-Corrected Scanning Transmission Electron Microscope. Microscopy and Microanalysis, 2012, 18, 711-719.	0.4	24
195	Tailoring the surface properties of LiNi _{0.4} Mn _{0.4} Co _{0.2} O ₂ by titanium substitution for improved high voltage cycling performance. Physical Chemistry Chemical Physics, 2015, 17, 21778-21781.	2.8	24
196	A general approach for the direct fabrication of metal oxide-based electrocatalysts for efficient bifunctional oxygen electrodes. Sustainable Energy and Fuels, 2017, 1, 823-831.	4.9	24
197	Dissolution of Pt during Oxygen Reduction Reaction Produces Pt Nanoparticles. Analytical Chemistry, 2017, 89, 12618-12621.	6.5	24
198	Ultrafine SmMn2O5-δ electrocatalysts with modest oxygen deficiency for highly-efficient pH-neutral magnesium-air batteries. Journal of Power Sources, 2020, 449, 227482.	7.8	24

#	Article	IF	CITATIONS
199	Channeling of a subangstrom electron beam in a crystal mapped to two-dimensional molecular orbitals. Physical Review B, 2012, 86, .	3.2	23
200	Synergic grain boundary segregation and precipitation in W- and W-Mo-containing high-entropy borides. Journal of the European Ceramic Society, 2021, 41, 5380-5387.	5.7	23
201	Pt skin on Pd–Co–Zn/C ternary nanoparticles with enhanced Pt efficiency toward ORR. Nanoscale, 2016, 8, 14793-14802.	5.6	22
202	Unusual strain effect of a Pt-based L1 _O face-centered tetragonal core in core/shell nanoparticles for the oxygen reduction reaction. Physical Chemistry Chemical Physics, 2019, 21, 6477-6484.	2.8	22
203	0.7 à Resolution Electron Tomography Enabled by Deepâ€Learningâ€Aided Information Recovery. Advanced Intelligent Systems, 2020, 2, 2000152.	6.1	22
204	Bulk high-entropy hexaborides. Journal of the European Ceramic Society, 2021, 41, 5775-5781.	5.7	22
205	Modification of the Coordination Environment of Active Sites on MoC for Highâ€Efficiency CH ₄ Production. Advanced Energy Materials, 2021, 11, 2100044.	19.5	21
206	Large-scale fabrication of field-effect transistors based on solution-grown organic single crystals. Science Bulletin, 2015, 60, 1122-1127.	9.0	20
207	Long-range ordering of composites for organic electronics: TIPS-pentacene single crystals with incorporated nano-fibers. Chinese Chemical Letters, 2017, 28, 2121-2124.	9.0	20
208	Charge Transport Modulation in PbSe Nanocrystal Solids by Au _{<i>x</i>} Ag _{1–<i>x</i>} Nanoparticle Doping. ACS Nano, 2018, 12, 9091-9100.	14.6	20
209	Rational synthesis and electrochemical performance of LiVOPO ₄ polymorphs. Journal of Materials Chemistry A, 2019, 7, 8423-8432.	10.3	20
210	Three-dimensional imaging of pore structures inside low-l̂º dielectrics. Applied Physics Letters, 2010, 96,	3.3	19
211	Bubble nucleation and migration in a lead–iron hydr(oxide) core–shell nanoparticle. Proceedings of the United States of America, 2015, 112, 12928-12932.	7.1	19
212	Achieving High Cycling Rates via In Situ Generation of Active Nanocomposite Metal Anodes. ACS Applied Energy Materials, 2018, 1, 4651-4661.	5.1	19
213	In Situ Visualization of Structural Evolution and Fissure Breathing in (De)lithiated H ₂ V ₃ O ₈ Nanorods. ACS Energy Letters, 2019, 4, 2081-2090.	17.4	19
214	Scalable synthesis of dispersible iron carbide (Fe3C) nanoparticles by â€~nanocasting'. Journal of Materials Chemistry A, 2019, 7, 19506-19512.	10.3	19
215	Analytical electron microscopy of black carbon and microaggregated mineral matter in Amazonian dark Earth. Journal of Microscopy, 2012, 245, 129-139.	1.8	18
216	Super-compression of large electron microscopy time series by deep compressive sensing learning. Patterns, 2021, 2, 100292.	5.9	18

#	Article	IF	CITATIONS
217	Hydrophobic Molecule Monolayer Brush-Tethered Zinc Anodes for Aqueous Zinc Batteries. ACS Applied Materials & Interfaces, 2021, 13, 60092-60098.	8.0	18
218	Atomic-level tunnel engineering of todorokite MnO2 for precise evaluation of lithium storage mechanisms by in situ transmission electron microscopy. Nano Energy, 2019, 63, 103840.	16.0	17
219	TEM-Assisted Fabrication of Sub-10 nm Scanning Electrochemical Microscopy Tips. Analytical Chemistry, 2019, 91, 15355-15359.	6.5	16
220	In Situ Visualization of Interfacial Sodium Transport and Electrochemistry between Few‣ayer Phosphorene. Small Methods, 2019, 3, 1900061.	8.6	15
221	Anomalously deep polarization in <mml:math xmlns:mml="http://www.w3.org/1998/Math/MathML"><mml:mrow><mml:mi>SrTi</mml:mi><mml:msub><mml:n mathvariant="normal">O<mml:mn>3</mml:mn></mml:n </mml:msub></mml:mrow> (001) interfaced with an epitaxial ultrathin manganite film. Physical Review B, 2016, 94, .</mml:math 	ni 3.2	14
222	Promoting the water dissociation of nickel sulfide electrocatalyst through introducing cationic vacancies for accelerated hydrogen evolution kinetics in alkaline media. Journal of Catalysis, 2022, 410, 112-120.	6.2	14
223	Determining On-Axis Crystal Thickness with Quantitative Position-Averaged Incoherent Bright-Field Signal in an Aberration-Corrected STEM. Microscopy and Microanalysis, 2012, 18, 720-727.	0.4	13
224	Periodic Artifact Reduction in Fourier Transforms of Full Field Atomic Resolution Images. Microscopy and Microanalysis, 2015, 21, 436-441.	0.4	13
225	Tailoring Surface Opening of Hollow Nanocubes and Their Application as Nanocargo Carriers. ACS Central Science, 2018, 4, 1742-1750.	11.3	13
226	Ligand-Assisted Solid-State Transformation of Nanoparticles. Chemistry of Materials, 2020, 32, 3271-3277.	6.7	13
227	Enhanced electrocatalytic activity and stability of Pd ₃ V/C nanoparticles with a trace amount of Pt decoration for the oxygen reduction reaction. Journal of Materials Chemistry A, 2015, 3, 20966-20972.	10.3	12
228	Visualizing the toughening origins of gel-grown calcite single-crystal composites. Chinese Chemical Letters, 2018, 29, 1666-1670.	9.0	12
229	Nanoscale x-ray and electron tomography. MRS Bulletin, 2020, 45, 264-271.	3.5	12
230	Solutionâ€Grown Organic Singleâ€Crystalline Donor–Acceptor Heterojunctions for Photovoltaics. Angewandte Chemie, 2015, 127, 970-974.	2.0	11
231	Direct observation of electronic-liquid-crystal phase transitions and their microscopic origin in La1/3Ca2/3MnO3. Scientific Reports, 2016, 6, 37624.	3.3	11
232	Nanoscale Origins of Ferroelastic Domain Wall Mobility in Ferroelectric Multilayers. ACS Nano, 2016, 10, 10126-10134.	14.6	11
233	Growth of Nanoparticles with Desired Catalytic Functions by Controlled Doping-Segregation of Metal in Oxide. Chemistry of Materials, 2018, 30, 1585-1592.	6.7	11
234	Dendritic Coreâ€Frame and Frame Multimetallic Rhombic Dodecahedra: A Comparison Study of Composition and Structure Effects on Electrocatalysis of Methanol Oxidation. ChemNanoMat, 2018, 4, 76-87.	2.8	11

#	Article	IF	CITATIONS
235	On the synthesis of bi-magnetic manganese ferrite-based core–shell nanoparticles. Nanoscale Advances, 2021, 3, 1612-1623.	4.6	11
236	Investigation of the multiplet features of SrTiO ₃ in X-ray absorption spectra based on configuration interaction calculations. Journal of Synchrotron Radiation, 2018, 25, 777-784.	2.4	10
237	In-situ TEM revisiting NH4V4O10 to unveil the unknown sodium storage mechanism as an anode material. Nano Energy, 2021, 87, 106182.	16.0	10
238	Intermediate selectivity in the oxidation of phenols using plasmonic Au/ZnO photocatalysts. Nanoscale, 2017, 9, 9359-9364.	5.6	8
239	Retrieving the energy-loss function from valence electron energy-loss spectrum: Separation of bulk-, surface-losses and Cherenkov radiation. Ultramicroscopy, 2018, 194, 175-181.	1.9	8
240	Highly Active and Stable Carbon Nanosheets Supported Iron Oxide for Fischerâ€Tropsch to Olefins Synthesis. ChemCatChem, 2019, 11, 1625-1632.	3.7	8
241	Pt–Ni Seed-Core-Frame Hierarchical Nanostructures and Their Conversion to Nanoframes for Enhanced Methanol Electro-Oxidation. Catalysts, 2019, 9, 39.	3.5	8
242	ALD growth of a mixed-phase novel barrier for seedless copper electroplating applications. , 2008, , .		7
243	A new spin on electron beams. Nature Nanotechnology, 2010, 5, 764-765.	31.5	7
244	Scanning Confocal Electron Energy-Loss Microscopy Using Valence-Loss Signals. Microscopy and Microanalysis, 2013, 19, 1036-1049.	0.4	7
245	Anomalous Growth Rate of Ag Nanocrystals Revealed by in situ STEM. Scientific Reports, 2017, 7, 16420.	3.3	7
246	Deep Learning Based Atom Segmentation and Noise and Missing-Wedge Reduction for Electron Tomography. Microscopy and Microanalysis, 2018, 24, 504-505.	0.4	7
247	Innenrücktitelbild: Atomically Dispersed Molybdenum Catalysts for Efficient Ambient Nitrogen Fixation (Angew. Chem. 8/2019). Angewandte Chemie, 2019, 131, 2547-2547.	2.0	7
248	Composition‶unable Antiperovskite Cu _{<i>x</i>} In _{1â^'<i>x</i>} NNi ₃ as Superior Electrocatalysts for the Hydrogen Evolution Reaction. Angewandte Chemie, 2020, 132, 17641-17646.	2.0	7
249	Probing Activities of Individual Catalytic Nanoflakes by Tunneling Mode of Scanning Electrochemical Microscopy. Journal of Physical Chemistry C, 2021, 125, 25525-25532.	3.1	7
250	Ultrafast Preparation of Nonequilibrium FeNi Spinels by Magnetic Induction Heating for Unprecedented Oxygen Evolution Electrocatalysis. Research, 2022, 2022, .	5.7	7
251	Fano resonance in atomic-resolution spectroscopic imaging of solids. Physical Review B, 2012, 86, .	3.2	6
252	Detection of magnetic circular dichroism in amorphous materials utilizing a single-crystalline overlayer. Physical Review Materials, 2017, 1, .	2.4	6

#	Article	IF	CITATIONS
253	Metal-Confined Synthesis of ZnS ₂ Monolayer Catalysts for Dinitrogen Electroreduction. ACS Catalysis, 2022, 12, 6809-6815.	11.2	6
254	Prospects for Reliable 3D Imaging in Aberration-corrected STEM, TEM and SCEM. Microscopy and Microanalysis, 2009, 15, 1474-1475.	0.4	5
255	Synergistic synthesis of quasi-monocrystal CdS nanoboxes with high-energy facets. Journal of Materials Chemistry A, 2015, 3, 23106-23112.	10.3	5
256	Combining post-specimen aberration correction and direct electron detection to image molecular structure in liquid crystal polymers. Microscopy and Microanalysis, 2016, 22, 1924-1925.	0.4	5
257	Quantification of Charge Transfer at the Interfaces of Oxide Thin Films. Journal of Physical Chemistry A, 2019, 123, 4632-4637.	2.5	5
258	Self-Limitations of Heat Release in Coupled Core-Shell Spinel Ferrite Nanoparticles: Frequency, Time, and Temperature Dependencies. Nanomaterials, 2021, 11, 2848.	4.1	5
259	Understanding growth mechanisms of epitaxial manganese oxide (Mn3O4) nanostructures on strontium titanate (STO) oxide substrates. MRS Communications, 2015, 5, 277-284.	1.8	4
260	In situ Studies of the Reaction-Driven Restructuring of Ni-Co Core-Shell Nanoparticles. Microscopy and Microanalysis, 2015, 21, 637-638.	0.4	4
261	Energy-loss- and thickness-dependent contrast in atomic-scale electron energy-loss spectroscopy. Physical Review B, 2014, 90, .	3.2	3
262	Correction to Porous Structured Ni–Fe–P Nanocubes Derived from a Prussian Blue Analogue as an Electrocatalyst for Efficient Overall Water Splitting. ACS Applied Materials & Interfaces, 2018, 10, 3152-3152.	8.0	3
263	High-Angular Splitting Electron Vortex Beams Generated by Topological Defects. Microscopy and Microanalysis, 2019, 25, 88-89.	0.4	3
264	Atomistic Defect Makes a Phase Plate for the Generation and High-Angular Splitting of Electron Vortex Beams. ACS Nano, 2019, 13, 3964-3970.	14.6	3
265	Atomic Modulation Engineering of Hexagon-Shaped CeO ₂ Nanocrystals by <i>In Situ</i> Sculpturing of an Electron Beam. Journal of Physical Chemistry C, 2020, 124, 17006-17014.	3.1	3
266	3D atomic imaging of low-coordinated active sites in solid-state dealloyed hierarchical nanoporous gold. Journal of Materials Chemistry A, 2021, 9, 25513-25521.	10.3	3
267	Contrasting Reaction Modality between Electrochemical Sodiation and Lithiation in NiO Conversion Electrode Materials. Microscopy and Microanalysis, 2015, 21, 325-326.	0.4	2
268	Hierarchical, Ultrathin Single-Crystal Nanowires of CdS Conveniently Produced in Laser-Induced Thermal Field. Langmuir, 2015, 31, 8162-8167.	3.5	2
269	Interfacial dislocations in (111) oriented (Ba0.7Sr0.3)TiO3films on SrTiO3single crystal. Applied Physics Letters, 2015, 107, 141605.	3.3	2
270	Artificial Intelligence Enabled Information Inpainting and Artifact Removal for Electron Tomography. Microscopy and Microanalysis, 2020, 26, 664-665.	0.4	2

#	Article	IF	CITATIONS
271	Electron Channeling Artifacts in Silicon [211] Using Aberration-Corrected STEM. Microscopy and Microanalysis, 2009, 15, 1492-1493.	0.4	1
272	Measurements of Porous Networks in Low-k Dielectric by Three-dimensional Electron Tomography. Microscopy and Microanalysis, 2009, 15, 1240-1241.	0.4	1
273	A Model Based Method for Tomographic Reconstructions of Nanoparticle Assemblies. Microscopy and Microanalysis, 2014, 20, 808-809.	0.4	1
274	Increasing the Dimensionality of In-situ Electron Microscopy Data Sets by On-the-fly and Analytical Electron Tomography. Microscopy and Microanalysis, 2016, 22, 724-725.	0.4	1
275	Modulation of Single-Atom Metal Sites for Enhanced Ambient Ammonia Electrosynthesis. Microscopy and Microanalysis, 2020, 26, 2794-2796.	0.4	1
276	AtomSegNet and TomoFillNet—Two Deep Learning Open-Source Apps for Superresolution Processing of Atomic Resolution Images and Missing-wedge Information Inpainting in Electron Tomograms. Microscopy and Microanalysis, 2020, 26, 926-926.	0.4	1
277	TEMImageNet, AtomSegNet and TomoFillNet, open-source libraries and models that enable defect localization in 2D and 3D atomic resolution images. Microscopy and Microanalysis, 2021, 27, 1456-1457.	0.4	1
278	Surface reconstruction and chemical evolution of stoichiometric layered cathode materials for lithium-ion batteries. , 0, .		1
279	Multicolor Photonic Pigments for Rotationâ€Asymmetric Mechanochromic Devices (Adv. Mater. 4/2022). Advanced Materials, 2022, 34, .	21.0	1
280	Image Contrast in Sub-Angstrom ADF-STEM. Microscopy and Microanalysis, 2007, 13, .	0.4	0
281	Prospects for Three-Dimensional, Sub-Nanometer Imaging with Aberration-Corrected ADF-STEM. Microscopy and Microanalysis, 2007, 13, .	0.4	0
282	Aberration-Corrected STEM Imaging and 2-D Elemental-Resolved Valence-EELS Mapping of Ru-TaN Ultrathin Barrier Layer. Microscopy and Microanalysis, 2009, 15, 1198-1199.	0.4	0
283	A 3-D Phase Evolution Panorama Uncovered Using a Grid-in-a-Coin Cell Method for Conversion Reaction Electrodes in Lithium-ion Batteries. Microscopy and Microanalysis, 2014, 20, 444-445.	0.4	0
284	Periodic Artifact Reduction in Fourier Transforms of Full Field Atomic Resolution Images. Microscopy and Microanalysis, 2015, 21, 2253-2254.	0.4	0
285	Toward 5D Imaging in an In-Situ Environmental TEM. Microscopy and Microanalysis, 2015, 21, 795-796.	0.4	0
286	Revealing Near-Surface to Interior Redox upon Lithiation in Conversion Electrode Materials Using Electron Microscopy. Microscopy and Microanalysis, 2015, 21, 1369-1370.	0.4	0
287	Detection of Magnetic Circular Dichroism in Amorphous Materials Utilizing a Single-Crystalline Overlayer. , 2016, , .		0
288	Quantification and Sensible Correction for Energy-Loss- and Thickness-Dependent Contrast Complications in Atomic-Scale Electron Energy-Loss Spectroscopy. Microscopy and Microanalysis, 2016, 22, 886-887.	0.4	0

#	Article	IF	CITATIONS
289	Towards a portable open-source tomography toolbox: Containerizing tomography software with docker. AIP Conference Proceedings, 2016, , .	0.4	0
290	Intricate Physics of Coherent Electron Beam/Oxide Materials Interaction Revealed by 4D Inline Holography—Electron Ptychography. Microscopy and Microanalysis, 2017, 23, 1632-1633.	0.4	0
291	Diagnostic Study of Lithium-Rich Cathode Materials at Primary and Sub-Primary Particle Level by Using Chemical-Sensitive STEM Tomography, Aberration-Corrected Imaging and EELS. Microscopy and Microanalysis, 2019, 25, 2056-2057.	0.4	0
292	Supercluster-Coupled Crystal Growth in Metallic Glass Forming Liquids. Microscopy and Microanalysis, 2019, 25, 1410-1411.	0.4	0
293	In-Situ Observation of Concurrent Oxidation and Mechanical Deformation in Al and Zr. Microscopy and Microanalysis, 2019, 25, 1912-1913.	0.4	0
294	Atomic-configuration Modulation of Active Sites on Electrocatalysts. Microscopy and Microanalysis, 2020, 26, 3014-3014.	0.4	0
295	Microscopy and Microanalysis 2020 Virtual. Microscopy Today, 2021, 29, 12-14.	0.3	0
296	(Invited) Electro-Chemo-Mechanical Degradation of LiNiO2-Derived High-Ni-Content Cathode Materials. ECS Meeting Abstracts, 2021, MA2021-01, 74-74.	0.0	0
297	Sodiation Kinetics of Metal Oxide Conversion Electrodes: A Comparative Study with Lithiation. ECS Meeting Abstracts, 2016, , .	0.0	0
298	Highly Efficient Nitrogen and Sulfur Co-Doped Three-Dimensional Graphene-Based Nanocatalysts for the ORR. ECS Meeting Abstracts, 2016, , .	0.0	0
299	Using New Quasi in-Situ TEM Technique to Study Structural Changes of Electrode Materials for Li-Ion and Na-Ion Batteries. ECS Meeting Abstracts, 2016, , .	0.0	0
300	Ultra-Low Amount of Pt Decorated Pd-Based Nanoparticles for the Oxygen Reduction Reaction. ECS Meeting Abstracts, 2016, , .	0.0	0
301	Important Roles of Crystallinity in Voltage Fade of Li- and Mn-Rich Cathodes Exemplified By Li2Ru0.5Mn0.5O3 Studies. ECS Meeting Abstracts, 2016, , .	0.0	0
302	Molybdenum-Based Nanomaterials As High Efficient Electrocatalysts for HER. ECS Meeting Abstracts, 2016, , .	0.0	0
303	Quantitative Nanostructure Analysis of Silver Vanadium Phosphorus Oxide (Ag2VO2PO4) Battery Material Using X-Ray and Electron Microscopy. ECS Meeting Abstracts, 2016, , .	0.0	0
304	Structural Stability of Nickel-Rich Layered Cathode Materials. ECS Meeting Abstracts, 2016, , .	0.0	0
305	Revealing Corrosion Chemistry in Lithium Ion Battery and Beyonda Tale of Two "Cities". ECS Meeting Abstracts, 2016, , .	0.0	0
306	Primary and Sub-Primary Particle Level Lithium Ion Battery Diagnostics Using Chemical-Sensitive STEM Tomography, Aberration-Corrected Imaging and Eels. ECS Meeting Abstracts, 2017, , .	0.0	0

#	Article	IF	CITATIONS
307	(Invited) Visualizing Electrochemical Reactions at the Nanoscale By in-Situ TEM. ECS Meeting Abstracts, 2017, , .	0.0	0
308	Scanning Spreading Resistance Microscopy (SSRM): High-Resolution 2D and 3D Carrier Mapping of Semiconductor Nanostructures. , 2017, , 419-488.		0
309	Investigation of Degradation Pathway in High Ni-Content Cathode Materials at Primary and Secondary Particle Level By Multi-Scale Characterization. ECS Meeting Abstracts, 2018, , .	0.0	0
310	(Invited) Evolution of Redox Couples in Li- and Mn-Rich Cathode Materials and Mitigation of Voltage Fade by Reducing Oxygen Release. ECS Meeting Abstracts, 2019, , .	0.0	0
311	X-Ray Induced Chemical Reaction Revealed by In Situ X-Ray Diffraction and Scanning X-Ray Microscopy in 15 nm Resolution. Journal of Electrochemical Energy Conversion and Storage, 2022, 19, .	2.1	0